Computers and Electronics in Agriculture 187 (2021) 106276

Contents lists available at ScienceDirect

Computers and Electronics in Agriculture

journal homepage: www.elsevier.com/locate/compag

Original papers

High resolution 3D terrestrial LiDAR for cotton plant main stalk and node detection

Shangpeng Sun [a,b], Changying Li [b,*], Peng W. Chee [c], Andrew H. Paterson [c,d], Cheng Meng [e,g], Jingyi Zhang [f,g], Ping Ma [g], Jon S. Robertson [d], Jeevan Adhikari [d]

[a] Department of Bioresource Engineering, Macdonald Campus, McGill University, Ste-Anne-de-Bellevue, QC, Canada
[b] Bio-Sensing and Instrumentation Laboratory, College of Engineering, Phenomics and Plant Robotics Center, the University of Georgia, Athens, GA, United States
[c] Department of Crop and Soil Sciences, College of Agricultural and Environmental Sciences, University of Georgia, Athens, GA, United States
[d] Department of Genetics, Franklin College of Arts and Sciences, University of Georgia, Athens, GA, United States
[e] Institue of Statistics and Big Data, Renmin University of China, Beijing, China
[f] Center for Statistical Science, Tsinghua University, Beijing, China
[g] Department of Statistics, Franklin College of Arts and Sciences, University of Georgia, Athens, GA, United States

ARTICLE INFO

Keywords:
High throughput phenotyping
Terrestrial LiDAR
Three-dimensional skeleton
Plant node detection
Minimum spanning tree

ABSTRACT

Dense three-dimensional point clouds provide opportunities to retrieve detailed characteristics of plant organ-level phenotypic traits, which are helpful to better understand plant architecture leading to its improvements via new plant breeding approaches. In this study, a high-resolution terrestrial LiDAR was used to acquire point clouds of plants under field conditions, and a data processing pipeline was developed to detect plant main stalks and nodes, and then to extract two phenotypic traits including node number and main stalk length. The proposed method mainly consisted of three steps: first, extract skeletons from original point clouds using a Laplacian-based contraction algorithm; second, identify the main stalk by converting a plant skeleton point cloud to a graph; and third, detect nodes by finding the intersection between the main stalk and branches. Main stalk length was calculated by accumulating the distance between two adjacent points from the lowest to the highest point of the main stalk. Experimental results based on 26 plants showed that the proposed method could accurately measure plant main stalk length and detect nodes; the average R^2 and mean absolute percentage error were 0.94 and 4.3% for the main stalk length measurements and 0.7 and 5.1% for node counting, respectively, for point numbers between 80,000 and 150,000 for each plant. Three-dimensional point cloud-based high throughput phenotyping may expedite breeding technologies to improve crop production.

1. Introduction

Crop improvement needs to increase at a faster pace due to a growing global population, climate change, and the limitations of natural resources such as arable land and water (Gerland et al., 2014; Tilman et al., 2011). To address this tremendous challenge, it is urgent to develop new technologies to accelerate plant breeding (Pieruschka and Schurr, 2019). Plant phenotyping measures and describes a diversity of phenotypic traits from cell to organ to the whole plant and assesses plant development and performance (Dhondt et al., 2013; Goggin et al., 2015; Ninomiya et al., 2019), which plays a vital role in accelerating the selection of new cultivars of crops to meet specific breeding and research goals and has become a rapidly-evolving area of focus in agricultural applications (Czedik-Eysenberg et al., 2018; Granier and Vile, 2014). Cotton (*Gossypium* spp.) is among the most economically important fiber crops, accounting for almost 79% of the total natural fiber production throughout the world (Fangueiro and Rana, 2016). Phenotypic traits of plant architectural traits such as main stalk length and nodes are useful to breeders and growers alike (Oosterhuis and Kerby, 2008). The traditional manual measurements of node related traits are time consuming and labor intensive. Therefore, high throughput phenotyping (HTP) methods of quantification of cotton plant architectural traits, especially noninvasive phenotyping in field conditions, are needed.

During the past decade, two-dimensional (2D) image-based methods were widely used in plant phenotyping applications, including crop growth monitoring (Li et al., 2014), disease detection (Ghosal et al.,

* Corresponding author at: 712F Boyd Graduate Studies, 200 D. W. Brooks Drive, University of Georgia, Athens, GA 30602, United States.
E-mail address: cyli@uga.edu (C. Li).

https://doi.org/10.1016/j.compag.2021.106276
Received 25 November 2020; Received in revised form 14 April 2021; Accepted 13 June 2021
Available online 30 June 2021

2018), and canopy size measurements (Wang et al., 2018). The emergence of deep learning technology (LeCun et al., 2015) greatly promotes the development of plant phenotyping, which offers the potential to provide generic solutions for plant image analysis (Singh et al., 2018; Tardieu et al., 2017). In order to better understand plant architecture leading to its improvements via new plant breeding approaches, efforts have been conducted to explore new imaging technologies to describe the characteristics of phenotypic traits at the organ level, such as leaf and stalk (Yin et al., 2018), flower (Xu et al., 2017) and fruit (Miller et al., 2017), and root analysis (Bao et al., 2018). One major challenge for image-based methods is the inherent occlusion, which is especially difficult to overcome under field conditions (Liu et al., 2019a). In addition, it is difficult to extract structure information from images, and image quality, which plays a vital role in trait detection performance, is hard to control under varied illumination conditions, thereby limiting its applications under field conditions (Gibbs et al., 2017; Jin et al., 2018).

Much effort has been made to explore three-dimensional (3D) methods for high throughput plant phenotyping (Vazquez-Arellano et al., 2016), and currently 3D-based methods are receiving increasing attention. Because on one hand, new sensor technologies and more powerful computers make dense point cloud collection and processing easier (Guo et al., 2018; Paulus et al., 2014); on the other hand, 3D data provide depth and structural information, which is highly useful for addressing occlusion, from which a wider variety of phenotypic traits can be retrieved (Gibbs et al., 2017). LiDAR is one of the most commonly used sensors for field-based phenotyping. Because LiDAR uses its own light source for distance measurement, it greatly reduces the impact on data quality caused by environmental illumination (Lin, 2015). 2D line scan LiDAR combined with GPS were often used to build plant 3D models under field conditions during the past decade; plot/plant level traits such as canopy size and plant volume were derived from the reconstructed point clouds (Auat Cheein et al., 2015; Méndez et al., 2016). However, because of limited resolution, it is difficult to retrieve plant organ level traits, such as those traits related to leaf, bloom, and fruit. The emergence of high-resolution LiDAR has enabled the creation of highly dense point clouds. Several attempts have been made to develop custom algorithms for the extraction of phenotypic traits using terrestrial LiDAR data for different types of plants, such as for sorghum panicle detection (Malambo et al., 2019), maize-stem size estimation (Jin et al., 2018), and grape leaf and stem segmentation (Paulus et al., 2013). Furthermore, stereo vision and structure from motion (SfM)-based methods have been used to reconstruct dense point clouds from images (Isokane et al., 2018; McCormick et al., 2016). These image-based methods can provide high quality point clouds under well-controlled environmental conditions, although limitations of 2D images related to varied illumination conditions still exist.

This study focused on cotton plant main stalk and node detection using a high-resolution LiDAR under field conditions. A node is the place where a branch joins with the main stalk (Fig. 1) (Corporation and Cottoninfo, 2019; Stewart et al., 2009). A cotton plant has an erect and prominent main stalk and consists of nodes and internodes. Two type of branches—vegetative and fruiting branches—are produced in a cotton plant. Vegetative branches arise from the main stalk near the ground, and the number depends primarily on environment and plant spacing. Fruiting branches, however, are produced primarily by a plant and produce fruits (cotton bolls). McCarthy et al. (2009) developed a vision system to detect cotton plant nodes from RGB images, in which nodes were identified by extracting line features of main stems and branches from acquired images. Although the absolute error of internode distance measurement for 95 detected nodes were small (6.1 mm), only around 11% (95 out of 840) nodes were detected. Visual occlusion was the main reason for nodes going undetected. Yamamoto et al. (2016) detected node and internode length of tomato plants from images under controlled environment, and image limitations with regard to occlusion is still difficult to overcome. Jin et al. (2018) introduced a median normalized-vector growth algorithm to segment stem and leaf of maize

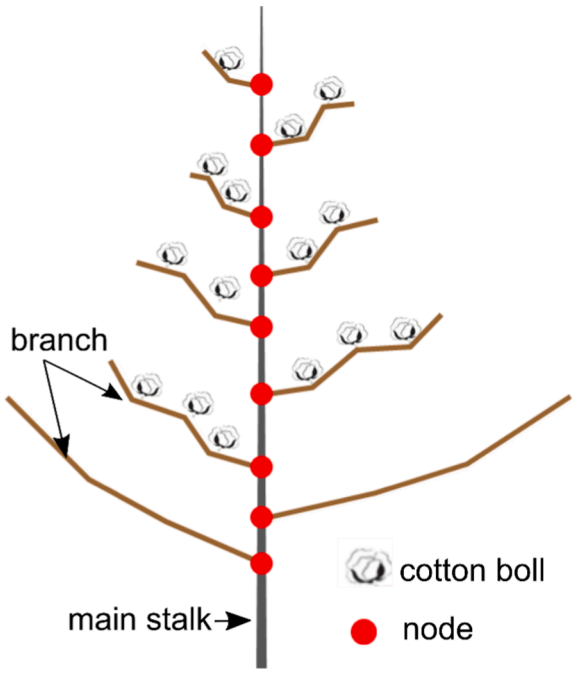

Fig. 1. Illustration of a general cotton plant architecture.

from point clouds and achieved an average segmentation accuracy of 93% for 30 samples, then phenotypic traits such as stem length and width, crown diameter and height were calculated. However, based on the review of phenotyping literature, 3D-based cotton plant node detection remains unexplored. Cotton plants have complex structures and their branches are long and dense. It is very likely that a branch crosses or is physically connected to other branches, posing challenges for node detection for cotton plants.

The overall goal of this study was to develop a 3D point cloud processing pipeline for field-based cotton plant main stalk detection and node counting using terrestrial LiDAR data. Specific objectives were to: (1) investigate the feasibility of applying a terrestrial LiDAR sensor to obtain plant point clouds under field conditions; (2) detect cotton plant main stalks using a Laplacian-based skeleton extraction algorithm and a graph-based approach; (3) detect plant nodes by finding the intersection between the main stalk and branches; (4) test the performance of the developed method using point clouds with different densities for two phenotypic traits (plant main stalk length and node number).

2. Material and methods

2.1. Experimental field and data collection

The experimental field was located at the Iron Horse Farm (latitude: 37.730 N, longitude: 83.303 W) in Greene County, GA, USA. There were in total 132 single cotton plants, 12 rows by 11 columns, with the plant inter-distance of approximate 152.4 cm (Fig. 2a). A 3D terrestrial LiDAR sensor (FARO Focus S70, FARO Technologies, USA) (Fig. 2b) mounted on a tripod at a height of approximately 1.0 m was used to scan plants to acquire point cloud data using a scanning point distance of 3.1 mm at 10 m. The sensor could conduct a 360° scan on the horizontal plane, so each plant could be scanned from four perspectives, while each scan could cover four plants (Fig. 2a). The scans were registered as point cloud datasets by the software, FARO SCENE, which was included with the sensor (Fig. 2c) and had a mean point error of 2 mm. The ground plane was removed using the tool provided by the SCENE software before exporting the point cloud data. Data collection was conducted on December 11 and 18, 2018, respectively. Fifteen plants were scanned on each day, resulting in a total of 30 point cloud datasets. The ground truth

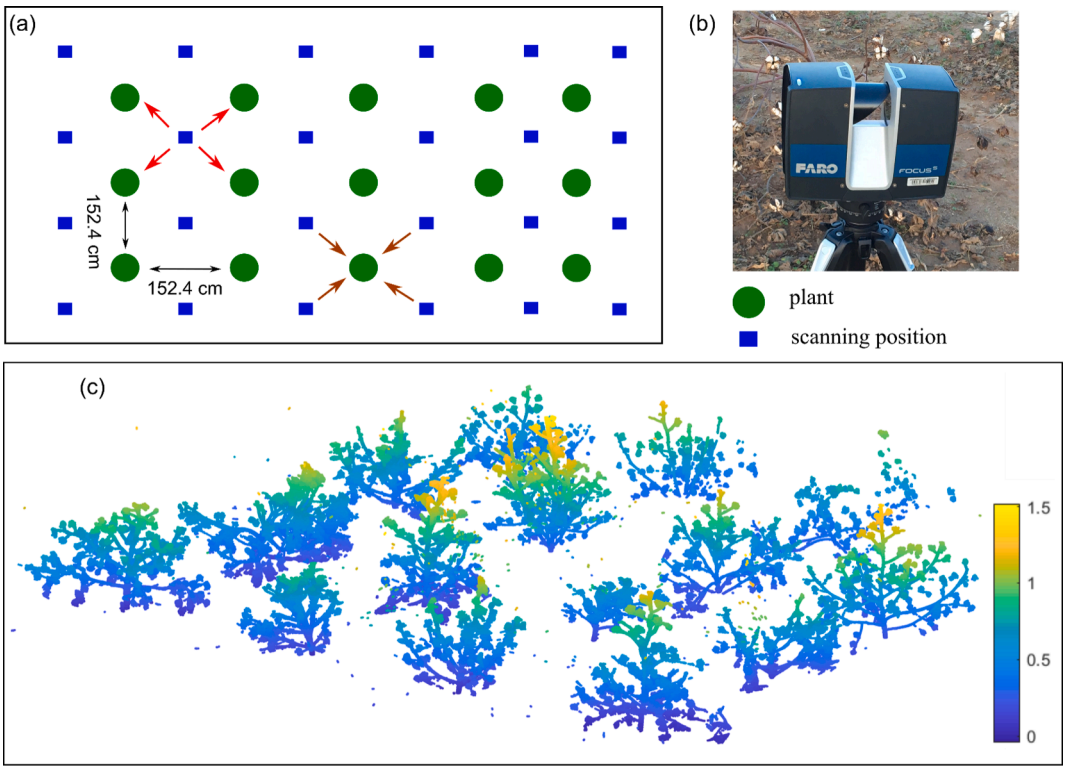

Fig. 2. Experimental field and scanned point cloud data using a terrestrial LiDAR. (a) Schematic of plant layout and scanning positions. (b) The LiDAR sensor used in this study. (c) Partial collected point cloud data.

data for two phenotypic traits—main stalk length and node number—were measured manually on the same day. Main stalk length was measured using a soft tape measure and node number was counted manually for each plant.

Highly accurate point clouds were obtained with the LiDAR using the proposed scanning strategy under field conditions (Fig. 3), from which plant organs such as branches and cotton bolls could be observed. The plants varied significantly in appearance because of environmental and genotypic factors. For this study, we observed plants with three basic types of plant architecture: typical upright cotton plants with erect stalks (Fig. 3a); slightly lodged plants with the main stalks moderately tilted (Fig. 3b); and severely lodged plants with the main stalks bent in several places such that some branches touched the ground (Fig. 3c). A cotton plant that is bent by chewing insects or heavy wind is known as lodging. The highest point of a plant was located at the main stalk in the first two categories. However, the severely lodged plants in the third category often have sustained damage; consequently, the highest points were located at one of the branches instead of at the main stalk for plants in the third category. For this study, we processed data only from plants in the first two categories (Fig. 3a and b).

2.2. Main stalk and node detection

Identification of the main stalk is a prerequisite for many plant organ level phenotypic trait measurements (Wang et al., 2018; Wu et al., 2019). A plant node is the part of the main stalk where branches start to grow, which can be detected by identifying the intersection between the main stalk and a branch (Fig. 4). The method for plant main stalk and node detection developed in this study mainly consisted of three steps: 3D skeleton extraction, main stalk detection, and node detection. Point cloud skeletonization is a thinning operation by which point cloud regions are reduced to lines that approximate their center lines. The purpose of skeletonization is to generate a thin, centered structure that maintains the topological and geometrical characterizations of the original point cloud data while greatly reducing data volume to facilitate further analysis (Tagliasacchi et al., 2016).

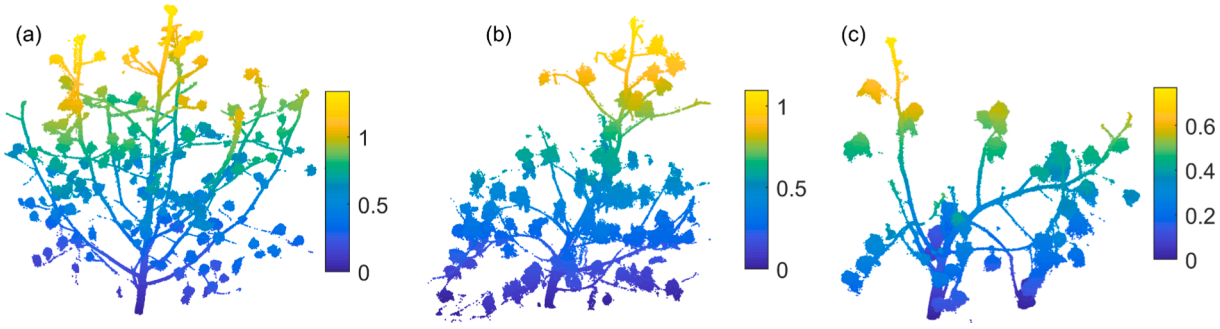

Fig. 3. Three categories of representative plants with different architectural patterns: (a) plants with an upright main stalk, and (b) and (c) plants with tilted main stalks. The highest point of (b) is located at the main stalk, while the highest point of (c) is located at a branch instead of at the main stalk.

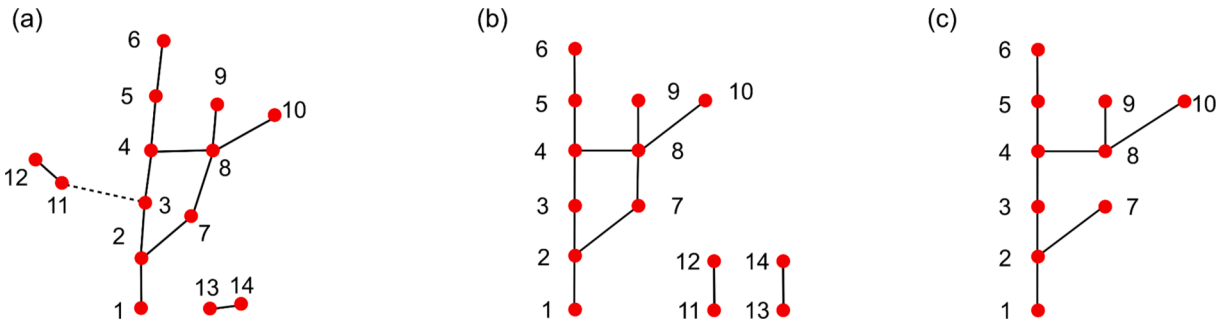

Fig. 4. Schematic of the algorithm for main stalk detection. (a) Example of the extracted skeleton points of a plant. The solid line means the two points are connected since the distance between them is so small (less a predefined threshold); the dashed line means the two points are not connected due to the large distance. (b) Graph converted from (a), in which three sub-graphs are included. Sub-graph 1 = {1, 2, 3, 4, 5, 6, 7, 8, 9, 10}, sub-graph 2 = {11, 12}, and sub-graph 3 = {13, 14}. (c) Minimum spanning tree converted from sub-graph 1 in (b), the lowest point (point 1) is selected, and starting from which, four paths are detected, they are path 1 = {1, 2, 3, 4, 5, 6}, path 2 = {1, 2, 7}, path 3 = {1, 2, 3, 4, 8, 9}, and path 4 = {1, 2, 3, 4, 8, 10}. Path 1 is selected as the main stalk because it contains the highest terminal point (point 6).

2.2.1. 3D skeleton extraction

A Laplacian-based contraction method was used to extract the plant curve skeleton from the point clouds because it is resistant to noise and can handle a moderate amount of missing data (Cao et al., 2010). Point clouds were denoised before feeding the skeleton extraction algorithm, and only point position information was used for skeletonization. Two steps were involved in this method, including geometric contraction and topological thinning. A point cloud could be contracted by iteratively solving the linear system (Eq. (1)).

$$\begin{bmatrix} W_L^t L^t \\ W_H^t \end{bmatrix} P^{t+1} = \begin{bmatrix} \mathbf{0} \\ W_H^t P^t \end{bmatrix} \tag{1}$$

where P^t was the point cloud for the t^{th} contraction operation, P^{t+1} was the corresponding point cloud after the contraction operation, and P^0 (t = 0) was the original point cloud with dimension of $n \times 3$, n was the number of points; L^t was a $n \times n$ Laplacian matrix which was constructed via 1-ring of a Delaunary triangulation; W_L^t and W_H^t were the $n \times n$ diagonal matrices, balancing the smoothness and similarity to the original points, respectively; $\mathbf{0}$ was a $n \times n$ zero matrix. $W_{L,i}^{t+1}$and $W_{H,i}^{t+1}$were updated using $W_{L,i}^{t+1} = S_L W_{L,i}^t$ and $W_{H,i}^{t+1} = W_{H,i}^0 S_i^0 / S_i^t$, respectively, where S_L was a constant coefficient, $S_L = 3$ was used following the suggestion in (Cao et al., 2010). $W_{L,\,i}^0 = 1/S_i^0$, $W_{H,\,i}^0 = 1$, and S_i^0 was the mean neighbor extent of point i in the point cloud; similarly, $S_i^t$was the mean neighbor extent of point i in the point cloud for the t^{th} repetition. The iteration of the contraction operation stopped when convergence achieved a steady state. The final contracted point cloud was denoted by C.

For the topological thinning operation, the contracted point cloud C was sampled using farthest point sampling (FPS) (Moenning and Dodgson, 2003) with a resolution of ε. FPS selects the lowest point in C as the starting point and iteratively selects the farthest point within a ball with a radius of ε from the previously selected points to produce a sampled dataset C′ from C. We then obtained the skeleton by imposing an initial connectivity on C′ and then collapsing unnecessary edges. The parameter ε was selected according to the size of interested traits. $\varepsilon = 5$ mm was used in this study since this value was so small that the extracted skeleton could distinguish nodes based on the observation of cotton plant internode distance. A down-sampling operation was conducted to reduce the point numbers to improve computational efficiency before performing the skeleton extraction. For clarity, it is important to distinguish between contraction and down-stamping. Contraction is an operation to shrink the shape of point clouds. It does not reduce the point numbers, while maintaining the key topological and geometrical features. Down-sampling is a thinning operation used to select some of the points from the original point clouds based on predefined rules. It reduces the point numbers but maintain the original shape.

2.2.2. Main stalk detection

A graph-based method was developed for main stalk detection, which involved two main steps: (1) initial main stalk points detection and (2) main stalk points refinement. The skeleton point set, denoted by $Pt = \{p_1, p_2, \cdots, p_k\}$, was divided into two sub-point sets: S and B. S was the main stalk point set, and B was a point set including all other points, $Pt = S \cup B, S \cap B = \varnothing$.

The initial main stalk points were detected by converting the skeleton points (Fig. 4a) to a graph (Fig. 4b) based on the 3D Euclidean distance between two points p_i and p_j (Eq. (2)). If the distance was less than a threshold λ which was selected based on the skeleton resolution ε, the two points were connected, such as point 1 and 2; otherwise, they were disconnected, such as point 3 and 11 (Fig. 4a). Each point in the generated graph was taken as a vertex and connected to its neighboring points with edges (Fig. 4b). The neighboring points are all those points whose 3D Euclidean distance to the given point is less than the predefined threshold λ. Three sub-graphs were included in Fig. 4b: sub-graph 1(sub-graph 1 = {1, 2, 3, 4, 5, 6, 7, 8, 9, 10}) contained most parts of the plant, resulting in the most number of points; sub-graph 2 (sub-graph 2 = {11, 12}) was created by part of a branch which did not connect to the main stalk because the minimum distance between point 11 and the main stalk points was greater than λ; sub-graph 3 (sub-graph 3 = {13, 14}) was created by materials laying on the ground, such as weeds or parts of the plant branches that were touching the ground. The main stalk points should be included in the sub-graph containing the most points (sub-graph 1 in Fig. 4b), which was selected for further processing. Then the selected sub-graph was converted to a minimum spanning tree (MST) (Tewarie et al., 2015) in order to cut circles in the graph (Fig. 4c), in which the lowest point (point 1) was selected, and starting from which, the standard shortest path search method was used to derive all paths in the MST. The path with the highest terminal point (point 6) was selected as the main stalk.

$$d(i,j) = \sqrt{(x_i - x_j)^2 + (y_i - y_j)^2 + (z_i - z_j)^2} \tag{2}$$

For the ideal situation in which there are no gaps in the skeleton (a gap means the distance between two adjacent points is greater than the predefined skeleton resolution ε), the parameter λ could be selected from the range (ε, 2ε) such that all main stalk points could be detected. However, gaps may exist in the skeleton because of incomplete point clouds although multi-view scanning was used for data collection in this study. In order to overcome the problem caused by potential gaps, λ should be a value slightly greater than the maximum gap distance in the initial main stalk detection step. The trajectory of a main stalk could be detected, but some points (points between two detected adjacent main stalk points in this step) belonging to the main stalk might not be detected.

The aim of the refinement operation was to detect these missed main stalk points according to the trajectory of pre-detected main stalk points. The method relied on the assumption that the main stalk within a short distance scale (λ) is a straight line. A line was formed between two adjacent pre-detected main stalk points, and the missed points located between the two pre-detected points should be very close to the line. In this study, a value of 3 mm was used to make a judgement whether a point belonged to the main stalk. If the distance between a point and the line was less than 3 mm, the point was considered to be a main stalk point and added to the main stalk point set *S*. Otherwise, it was a branch point.

2.2.3. Node detection

A node can be detected by identifying the intersection between the main stalk and a branch. Therefore, after the main stalk was detected, individual branches needed to be identified. A 'pruning' operation was designed to cut parts of branches which were far away from the main stalk before identifying each branch in order to simplify plant structures. First, circles were set with the same radius *r* along the main stalk starting from the lowest point in the crown to the highest point (Fig. 5a); second, points outside of the circles were removed. Thus, a short part of each branch close to the main stalk was kept, resulting in a simpler branch structure (Fig. 5b). After that, 3D density-based spatial clustering of applications with noise (DBSCAN) was applied on the remaining branch points, from which the output clusters were individual branches.

To detect a node, 3D Euclidean distances between points in a branch cluster $b = \{b_1, b_2, \cdots, b_n\}$ and a main stalk point set $S = \{s_1, s_2, \cdots, s_m\}$ were calculated, generating a distance matrix table (Table 1). s_{iz} was the value on the z axis for stalk point s_i; $d(s_i, b_j)$ denoted the distance between point s_i and b_j; d_{si} was the minimum distance between point s_i and points in the branch cluster *b*. An example of visualization for Table 1 was shown in Fig. 6b, in which black dots were the distance point pairs (s_{iz}, $d(s_i, b_j)$) and the blue line consisted of point pairs (s_{iz}, d_{si}) where d_{si} is the minimum distance between s_i *and* b_j. Local minimum peak points of the blue line were then detected, denoted by $N_i = (s_{Ni}, d_{Ni})$. If the vertical axis value d_{Ni} was small enough ($d_{Ni} < \tau_1$) (Fig. 6b), it indicated that there was a node in *s*, and the value of the node on z-axis was s_{Ni}. Accordingly, the corresponding node could be identified in *s*. The parameter τ_1 was used to check whether the distance between the main stalk and a branch was so large that the position of the detected node needed to be adjusted. $\tau_1 = 1$ cm was used in this study considering that the skeleton resolution was 5 mm.

For the situation demonstrated in Fig. 6c, a gap existed between the main stalk and a branch, i.e., the vertical axis value of the peak point was greater than τ_1 (Fig. 6d). A pseudo node could be found in the corresponding point set *s* using the method described for the situation shown in Fig. 6a and b, However, the actual node should be located below the pseudo node (Fig. 6c). The actual node location could be estimated using the following method: a line was fit for the branch points, and then a point in *s* having the shortest distance to the line was selected as the actual node.

Table 1
Distance matrix between the main stalk and a branch cluster.

	b_1	b_2	…	b_n	min($d(s_i, b_j)$)
s_{1z}	$d(s_1, b_1)$	$d(s_1, b_2)$	…	$d(s_1, bn)$	d_{s1}
s_{2z}	$d(s_2, b_1)$	$d(s_2, b_2)$	…	$d(s_2, b_n)$	d_{s2}
⋮	⋮	⋮	…	⋮	⋮
s_{mz}	$d(s_m, b_1)$	$d(s_m, b_2)$	…	$d(s_m, b_n)$	d_{sm}

For the situation two or more peak points were detected (Fig. 6e and f), a *k*-means clustering method with $k = 2$ was applied to reduce the number of peak points to two. Then, for each peak point, the method described for the situations in Fig. 6a and c was used to identify the node position in *s*. $k = 2$ was used because misclustering of 3D DBSCAN happened mostly with two close branches based on observation. If the vertical axis value of a peak point was greater than $\tau_2 = 3$ cm, the point would not be further analyzed because it was very likely caused by noisy points

The data processing algorithm was developed and implemented in software MATLAB 2018a (The Math Works Inc., Natick, MA, USA) on a desktop equipped with an Intel i7-6700 K CPU 4.00 GHz with 16G RAM, running an operating system of Windows 10 Pro.

2.3. Plant architecture traits measurements and accuracy validation

After plant main stalk and nodes were detected, two plant architecture traits, including plant node number and main stalk length, were extracted. The node number was obtained by counting all detected nodes. Main stalk length was calculated by accumulating the distance between two adjacent points of the whole main stalk skeleton points starting from the lowest point of the crown (Eq. (3)).

$$L = \sum_{i-1}^{M-1} d(i, i+1) \tag{3}$$

where *L* was the main stalk length, *M* was the point number of the main

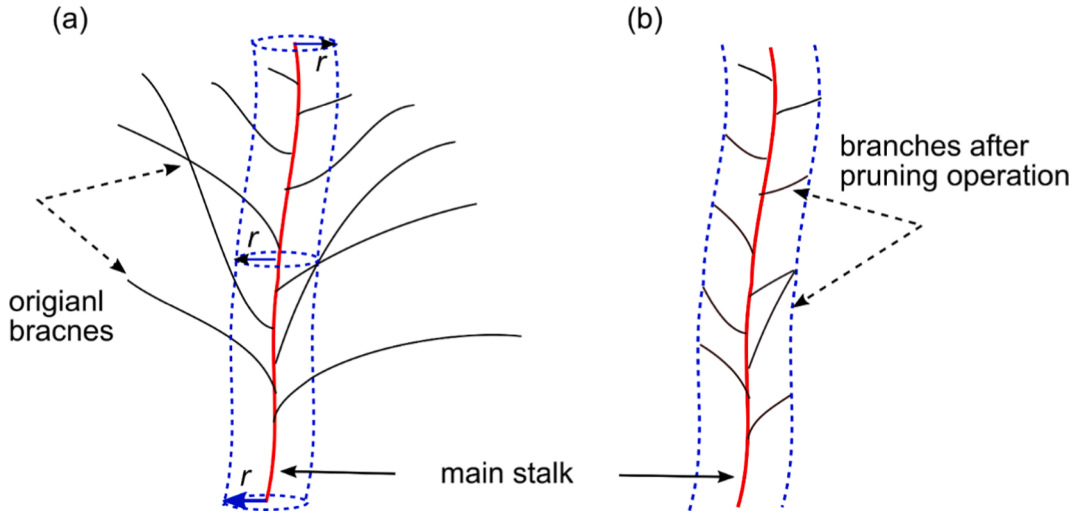

Fig. 5. Schematic of branch pruning operation. (a) Circles were set with the same radius *r* along the main stalk starting from the lowest point in the crown to the highest point. (b) Branches after pruning operation.

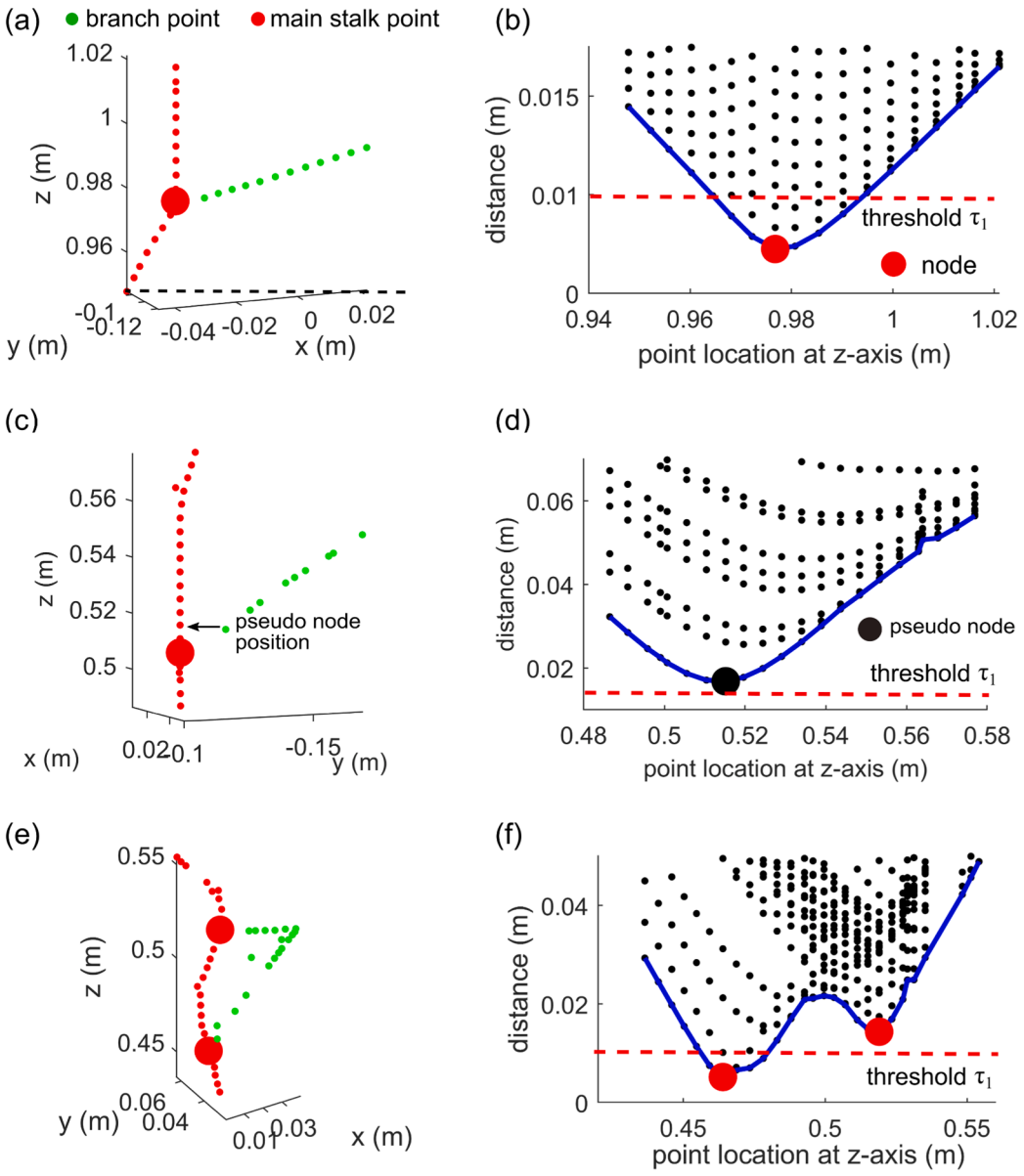

Fig. 6. Schematic for the node localization algorithm. For situation (a), the branch was connected to the main stalk, the point (b) in the main stalk with minimum distance was considered to be the node; For situation (c), there was a gap between the main stalk and a branch, and the real node (d) was below the point with minimum distance. For situation (e), two local low peaks were detected, and the corresponding distance was less than the distance threshold, so the two nodes could be detected.

stalk and $d(i, i+1)$ was the Euclidean distance between point i and $i+1$. For plant node number counting, the mean absolute percentage error (*MAPE*) was computed between the algorithm measuring node numbers N_i and the manual measurements m_i by Eq. (4). P was the number of plants.

$$MAPE = \frac{\sum_{i=1}^{P} \frac{|N_i - m_i|}{m_i}}{P} \times 100\% \quad (4)$$

In addition, the coefficient of determination (R^2) was calculated to assess the performance. These two metrics were also used to assess the other phenotypic traits. The method's performance was tested with different point cloud densities of 50,000, 80,000, 120,000, and 150,000 points for each plant.

3. Results

3.1. Skeleton extraction and main stalk detection

Overall, the extracted skeletons matched well with the original point clouds (Fig. 7), maintaining plants topological and geometrical features while greatly reducing point numbers. In this study, a single plant had around 3 ~ 6 million points, while the skeleton had around 2 ~ 5 thousand points depending on the plant size. As demonstrated in Fig. 7a, b and c, a branch was represented by a line of points in the extracted skeleton dataset. Although, the crown could be simply detected by selecting the lowest point of the skeleton, as shown in Fig. 7a and b, this would not work for the situation as shown in Fig. 7c. Some skeleton points inside the red ellipse in Fig. 7c, which were generated by any branch touching the ground, might have the same lowest height as the crown. In the proposed graph-based method, the points in the red ellipse could easily be removed based on the number of points for each sub-

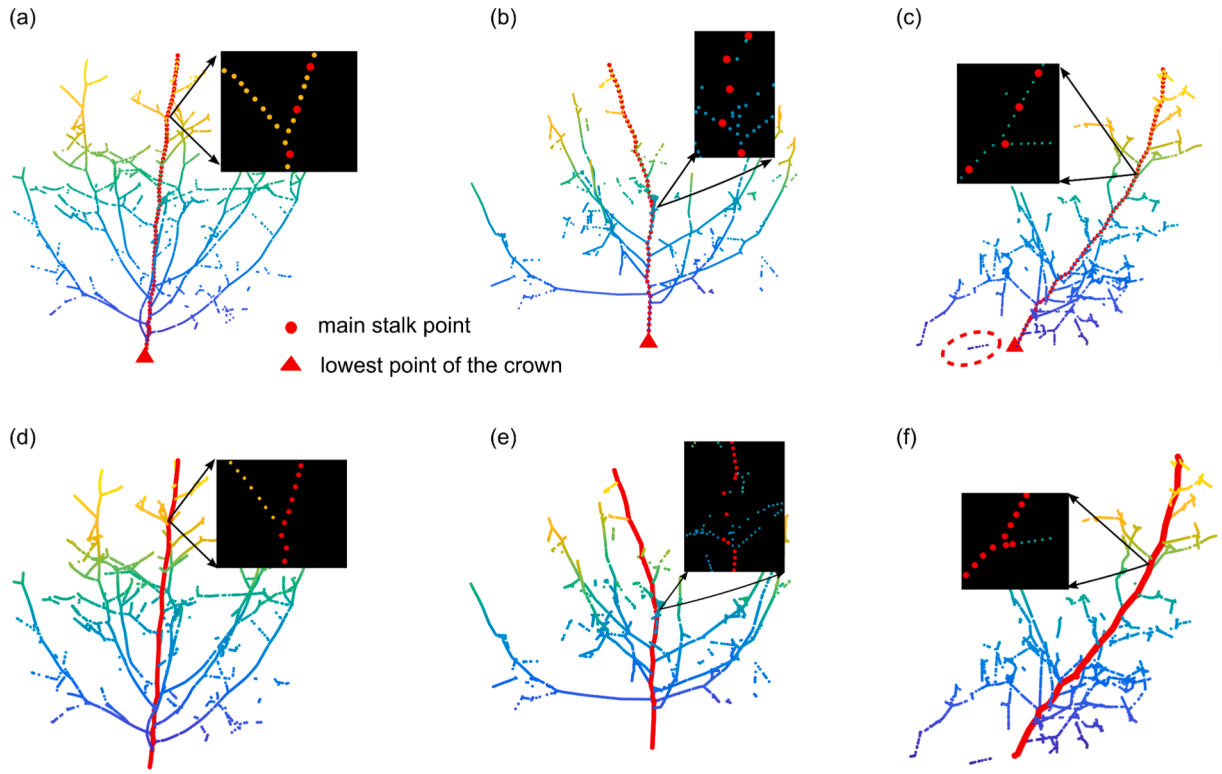

Fig. 7. Extracted skeletons and main stalk detection results. The first row demonstrated the extracted skeletons, the lowest points of crowns (indicated by red triangles) and initial main stalk points (indicated by red dots) detection results. (a) Skeleton of a plant with a straight upward main stalk. (b) Skeleton of a plant with a tilted main stalk; gaps existed in the main stalk skeleton points. (c) Skeleton of a plant with a tilted main stalk, part of the branch skeleton points was at the same height as the root point. The second row ((d), (e) and (f)) demonstrated the main stalk detection results after refinement operation. (For interpretation of the references to color in this figure legend, the reader is referred to the web version of this article.)

graph.

The main stalk could be reached by laser beams from all scanning perspectives; therefore, the occluded areas were small, resulting in small gaps in the main stalk skeleton (Fig. 7b). Based on this observation, the parameter λ, which was used to convert the skeleton points into a graph, was set to be 2 cm for the step of initial main stalk point detection, and results showed that this setting was large enough to cover all gaps. For the well-extracted main stalk skeleton (no gaps existed), there were three skeleton points between two adjacent pre-detected main stalk points, as demonstrated in the zoomed-in figures in Fig. 7a and c, because $\varepsilon = 5$ mm was used for skeleton extraction. Results of the main stalk points refinement operation showed that main stalk points were successfully detected for all plants. However, some branch points might be assigned to the main stalk point sets (Fig. 7f). This would not affect the presence of node detection, but would cause the detected node location to shift. More discussion was presented in Section 3.2.

3.2. Individual branch identification and node detection

Branch structure became much simpler compared to the original situation after the pruning operation (Fig. 8). We found that the circle radius r was flexible; experimental results showed the value did not affect the results much when it was selected in a range of 10–20 cm. In this study, the circle radius r was set to be 15 cm. The parameters *Eps* and *MinPts* of DBSCAN clustering algorithm were selected as 2 cm and 3, respectively, for the individual branch identification, considering the skeleton resolution configuration and potential skeleton gap size. Results showed that most of the 'pruned' branches were successfully grouped into different clusters. However, it was observed that a branch might be divided into different clusters due to the gaps (Fig. 8a), and

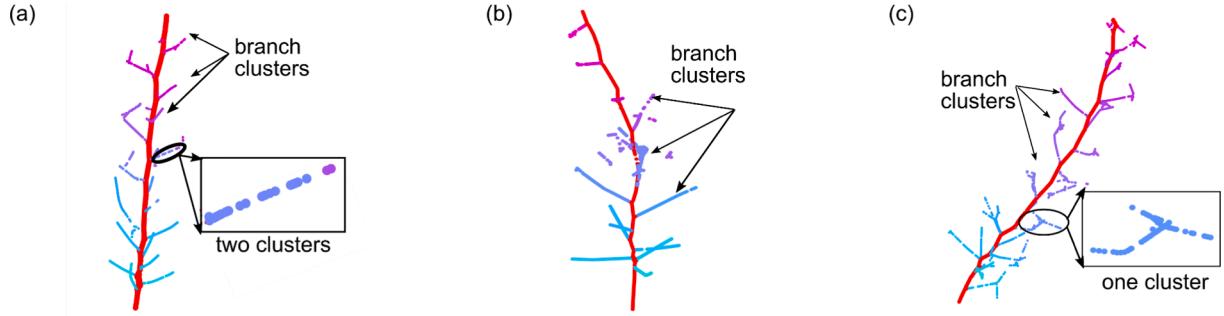

Fig. 8. Individual branch identification results for the two kinds of representative plant architectures. (a) A plant with a straight upward main stalk; (b) and (c) Plants with tilted main stalks. The main stalk points were indicated in red. For branches, each color represented a detected branch cluster. (For interpretation of the references to color in this figure legend, the reader is referred to the web version of this article.)

branches which were too close to each other would be grouped in the same cluster (Fig. 8c). These misclustering results were addressed by the node detection method described in Fig. 6.

Overall, the proposed node detection method performed well to identify nodes for plants with normal (Fig. 9a) and tilted main stalks (Fig. 9b and c). Usually, nodes at the lower part of a plant were denser than those located at a higher level. The proposed method was able to distinguish them due to the skeleton resolution configuration (Fig. 9a). In the case that a branch was divided into two or more clusters (Fig. 8a), the cluster which was far away from the main stalk could be removed using the distance filter ($\tau_2 = 3$ cm); For the situation demonstrated in Fig. 7f, a node was detected, but the location was shifted a few points (Fig. 7c). This was one of the limitations for the main stalk points detection.

3.3. Validation of extracted plant architecture traits

The performance of the method developed to calculate plants' main stalk length and node number was stable when the number of points for a plant was greater than 80,000 (Fig. 10). The average R^2 and MAPE for the plant's main stalk length were 0.94 and 4.3%, respectively, for point numbers between 80,000 and 150,000. Specifically, for the plant's main stalk length, the performance did not decrease when the number of points was reduced to 50,000, which indicates that the plant's main stalks were detected successfully. The average R^2 and MAPE for the node numbers were 0.70 and 5.1%, respectively, for point numbers between 80,000 and 150,000, while the performance decreased significantly when the point number was 50,000. We could not obtain point clouds for branches as dense as that of the main stalks because branches could not be scanned from four different directions and were thinner than the main stalk.

4. Discussion

Highly accurate point clouds of plants can be obtained using the 3D LiDAR with multi-view scanning strategy under field conditions, which provide a detailed and precise representation of plants, enabling retrieving plant phenotypic traits at both the whole plant level and organ level (Dhondt et al., 2013). The multi-view scanning strategy greatly reduces the possibility of occlusion, which is one of the biggest challenges for phenotypic trait extraction from 2D images. However, one limitation is that it takes a relatively long time for data collection. Therefore, scanning positions will be optimized in the future, keeping the quality and density of point clouds while reducing the number of scanning positions. For example, a plant can be scanned from fewer perspectives, such as three (each scan covering 120°) or even two (each scan covering 180°); another potential solution would be to mount the LiDAR at a higher position so that it can cover a larger field area (more plants) (Malambo et al., 2019; Wu et al., 2019), while configuring the sensor at a higher scanning resolution to achieve the same level of accuracy. Furthermore, the sensor can be mounted on a GPS-navigated robot platform, and point cloud registration operation can be conducted while collecting data. An efficient data collection method would be extremely useful for large field applications.

Overall, the skeleton extraction method performed well for cotton plants which had wide variation in appearance of the architecture, although there existed small gaps. In order to address the issue of gaps existing in the skeletons, a parameter λ, which was four times larger than the skeleton resolution, was used for the main stalk detection to ensure that two coarse adjacent connected points in the graph can cover the gaps. Gaps also exist between a branch and the main stalk as shown in Fig. 6c, specific algorithms were proposed to overcome the problem. If the skeleton could be well-extracted (no gaps would exist), the proposed main stalk and node detection method could become simpler. For example, the main stalk detection could be implemented just by the first step via setting the parameter λ as a value in the range of (ε, 2ε). The node position would not be affected by the gaps between a branch and the main stalk described in Fig. 6c and Fig. 7f. Therefore, future work will focus on optimization of the skeleton extraction algorithm. New algorithms will be developed to retrieve skeletons from incomplete point clouds. Structure patterns of the visible branches can be used to predict branch growth direction in order to fill out gaps (Li and Wang, 2018; Mei et al., 2016). A point cloud down-sampling method can also contribute to improve skeleton quality. In this study, the original point clouds were down-sampled using a random sampling method. For small stem branches, which generate fewer points than big ones, the point number may be too small to extract a fine skeleton after the down-sampling operation. If the down-sampling operation was conducted based on point density information, i.e., a branch which has a low density of points, fewer points would be removed during the down-sampling operation; otherwise, more points are removed. This down-sampling method could result in a more evenly distributed point cloud, which is good for skeleton extraction.

With regard to node detection, it was observed that the method produced a higher FN rate than FP rate. FN was mainly attributed to the situation that there was a big gap between a branch and the main stalk skeleton points (Fig. 11a, b and c). Some branches, especially those located at the top of a plant, were of a small stem diameter, resulting in less points in the original point cloud compared to those with a larger stem diameter. After down-sampling, the full skeleton of the branches with a small stem diameter might not be retrieved if they generate a very limited number of points. Fig. 11d demonstrated a representative situation for FP node detection. There was a sub-branch, which was close to the main stalk, and ghost points appeared due to the point cloud registration operation and environmental factors such as wind, resulting in the corresponding branch skeleton points being very close to the main stalk (Fig. 11e). The node detection method would detect this as a node (Fig. 11f). Because wind affects point cloud data randomly, it is difficult to remove all ghost points although denoising preprocessing was applied.

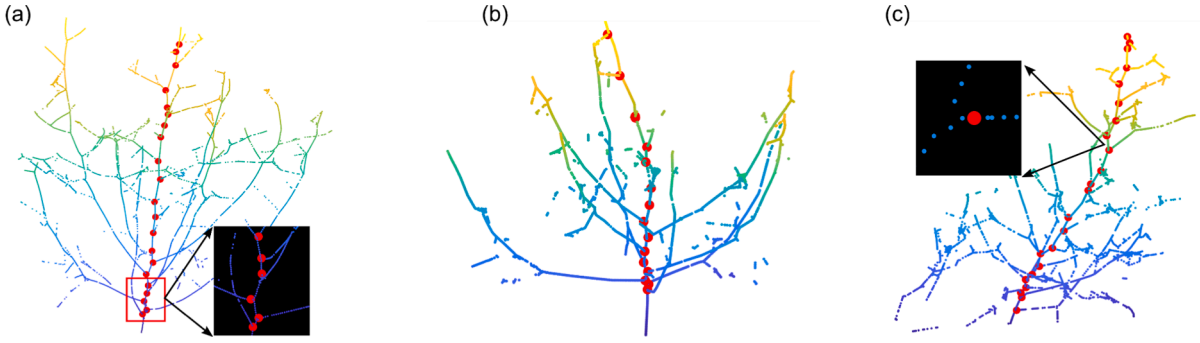

Fig. 9. Representative results of node detection. (a) A plant with normal architecture; (b) and (c) Plants with tilted main stalks. Detected nodes are indicated in red. (For interpretation of the references to color in this figure legend, the reader is referred to the web version of this article.)

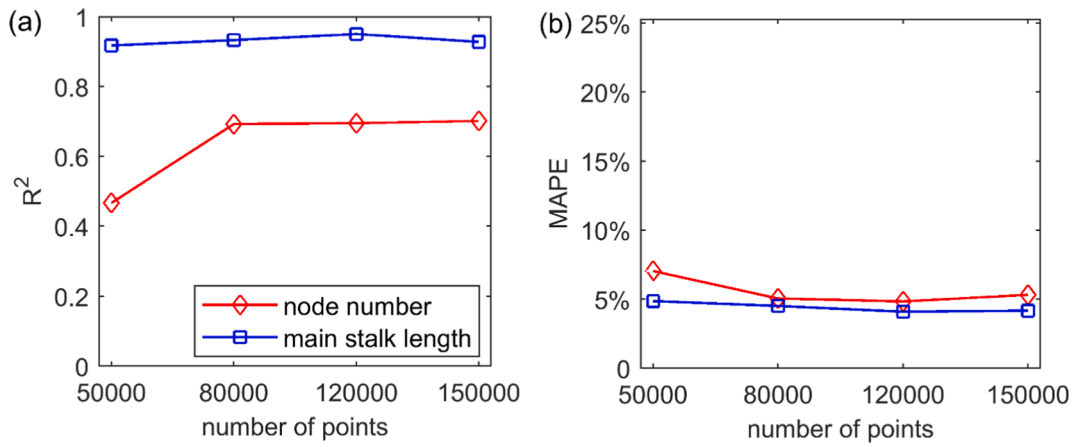

Fig. 10. Performance (a) R^2 value and (b) mean absolute percentage error for the main stalk length measurement and node number counting at different point cloud densities.

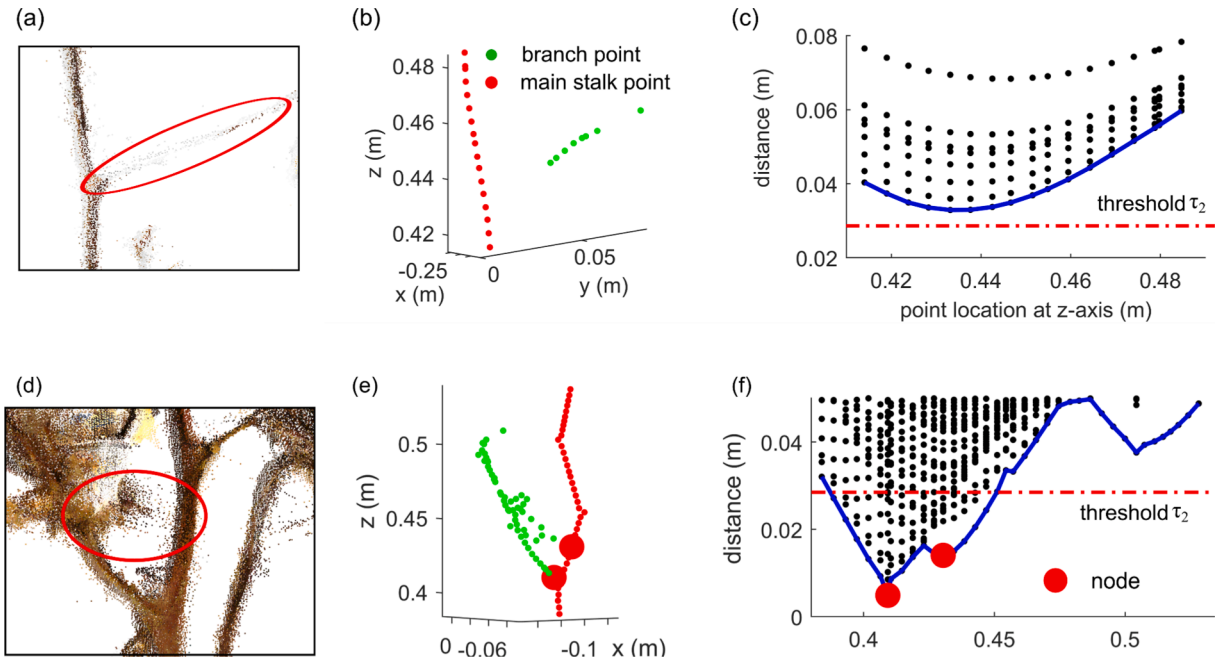

Fig. 11. Error analysis for false negative and false positive node detection. The first row is to demonstrate FN. Incomplete point cloud for a branch in (a). For the skeleton, there is a gap between the branch and the main stalk (b). The smallest distance is greater than the outliner threshold (c), resulting in a missing node. The second row is to demonstrate FP. The sub-branch is almost connected to the main stalk due to noisy points in (d). For the skeleton (e), although there is a small gap, it is less than the distance threshold, so two nodes are detected (f).

Results shown in Fig. 9 and Fig. 10 indicated that main stalk points were successfully detected using the proposed method which overcame the gap problem in the skeleton points. Another limitation of the main stalk detection method is that it is designed only for when the highest point of the plant is at the main stalk. However, some plants may not satisfy this requirement. For example, a plant may lodge because of wind or other environmental factors, which could result in one of the branches being the highest point, as demonstrated in Fig. 3c. The main stalk detection method will be optimized in the future. One potential solution is to apply 3D deep learning methods (Liu et al., 2019b; Qi et al., 2019), which can extract features in complex object detection more effectively.

In addition to the traits extracted in this study, more traits can be extracted from the point cloud data. For example, if whole branches, not just part of them as in this study, could be identified, combined with cotton boll detection technology (Sun et al., 2018), information as to where each cotton boll is located on each branch could be obtained. Branch angle (the angle between a branch and the main stalk) also could be estimated from the skeleton. A plant with average, small branch angles indicates that the plant architecture exhibits more upright branches, producing a more compact shape. This is helpful to increase plant density and improve final yield (Tian et al., 2019). Other traits such as canopy size and plant volume could also be detected. New algorithms will be developed for these traits.

5. Conclusions

In this study, highly accurate point cloud data were obtained using a high-resolution terrestrial 3D LiDAR sensor, thus enabling the retrieval of plant organ level phenotypic traits. The extracted skeleton greatly reduced point cloud data volume meanwhile maintained the topological and geometric patterns. Based on the skeleton point clouds, plant main stalks and nodes were accurately detected. We tested the algorithm

developed with different point cloud densities, and results demonstrate that the plant's main stalk length and node number could be detected accurately with stable performance when the point number was greater than 80,000 for each plant. In the future, new scanning strategies that require fewer scans without sacrificing accuracy will be explored to save field data collection time, and new algorithms will be developed to retrieve more traits from point clouds.

Declaration of Competing Interest

The authors declare that they have no known competing financial interests or personal relationships that could have appeared to influence the work reported in this paper.

Acknowledgement

This work was partially supported by the National Robotics Initiative grant (NIFA grant No. 2017-67021-25928), the Growing Converngence Research program (NSF grant No. 1934481), Cotton Incorporated (17-510GA), and Presidential Interdisciplinary Seed Grant at the University of Georgia.

The authors gratefully thank Rikki Brown and Piyush Pandey for their assistance in point cloud data collection.

Author contributions

S.S, C.L and P.W.C conceived the idea and designed the experiments; A.H.P and P.W.C contributed to the preparation of materials and equipment; S.S, J.S.R, and J.A conducted the experiments; S.S and C.M analyzed the data; S.S, C.L, A.H.P, P.W.C and P.M interpreted results and wrote the paper. All authors read and approved the final manuscript.

References

Auat Cheein, F.A., Guivant, J., Sanz, R., Escolà, A., Yandún, F., Torres-Torriti, M., Rosell-Polo, J.R., 2015. Real-time approaches for characterization of fully and partially scanned canopies in groves. Comput. Electron. Agric. 118, 361–371.

Bao, T., Melenka, G.W., Ljubotina, M.K., Carey, J.P., Cahill, J.F., 2018. A new method for the rapid characterization of root growth and distribution using digital image correlation. New Phytol. 218, 835–846.

Cao, J., Tagliasacchi, A., Olson, M., Zhang, H., Su, Z., 2010. Point cloud skeletons via laplacian based contraction, IEEE Shape Modeling International (SMI 2010), pp. 187–197.

Corporation, C.R.a.D., Cottoninfo, 2019. Australian Cotton Production Manual 2019.

Czedik-Eysenberg, A., Seitner, S., Guldener, U., Koemeda, S., Jez, J., Colombini, M., Djamei, A., 2018. The 'PhenoBox', a flexible, automated, open-source plant phenotyping solution. New Phytol. 219, 808–823.

Dhondt, S., Wuyts, N., Inze, D., 2013. Cell to whole-plant phenotyping: the best is yet to come. Trends Plant Sci. 18, 433–444.

Fangueiro, R., Rana, S., 2016. Natural fibres: advances in science and technology towards industrial applications. Springer, Netherlands, Dordrecht.

Gerland, P., Raftery, A.E., Ševčíková, H., Li, N., Gu, D., Spoorenberg, T., Alkema, L., Fosdick, B.K., Chunn, J., Lalic, N., 2014. World population stabilization unlikely this century. Science 346, 234–237.

Ghosal, S., Blystone, D., Singh, A.K., Ganapathysubramanian, B., Singh, A., Sarkar, S., 2018. An explainable deep machine vision framework for plant stress phenotyping. Proc. Natl. Acad. Sci. U. S. A. 115, 4613–4618.

Gibbs, J.A., Pound, M., French, A.P., Wells, D.M., Murchie, E., Pridmore, T., 2017. Approaches to three-dimensional reconstruction of plant shoot topology and geometry. Funct. Plant Biol. 44, 62–75.

Goggin, F.L., Lorence, A., Topp, C.N., 2015. Applying high-throughput phenotyping to plant–insect interactions: picturing more resistant crops. Curr. Opin. Insect Sci. 9, 69–76.

Granier, C., Vile, D., 2014. Phenotyping and beyond: modelling the relationships between traits. Curr. Opin. Plant Biol. 18, 96–102.

Guo, Q., Wu, F., Pang, S., Zhao, X., Chen, L., Liu, J., Xue, B., Xu, G., Li, L., Jing, H., 2018. Crop 3D — a LiDAR based platform for 3D high-throughput crop phenotyping. Sci. China Life Sci. 61, 328–339.

Isokane, T., Okura, F., Ide, A., Matsushita, Y., Yagi, Y., 2018. Probabilistic plant modeling via multi-view image-to-image translation. In: Proceedings of the IEEE Conference on Computer Vision and Pattern Recognition, pp. 2906–2915.

Jin, S., Su, Y., Wu, F., Pang, S., Gao, S., Hu, T., Liu, J., Guo, Q., 2018. Stem-leaf segmentation and phenotypic trait extraction of individual maize using terrestrial LiDAR data. IEEE Trans. Geosci. Remote Sensing 57, 1336–1346.

LeCun, Y., Bengio, Y., Hinton, G., 2015. Deep learning. Nature 521, 436–444.

Li, L., Wang, W., 2018. Improved Use of LOP for Curve Skeleton Extraction. Comput. Graphics Forum 37, 313–323.

Li, L., Zhang, Q., Huang, D.F., 2014. A review of imaging techniques for plant phenotyping. Sensors 14, 20078–20111.

Lin, Y., 2015. LiDAR: An important tool for next-generation phenotyping technology of high potential for plant phenomics? Comput. Electron. Agric. 119, 61–73.

Liu, S., Martre, P., Buis, S., Abichou, M., Andrieu, B., Baret, F., 2019a. Estimation of plant and canopy architectural traits using the D3P Digital Plant Phenotyping Platform. Plant Physiol. 881–890.

Liu, Z., Tang, H., Lin, Y., Han, S., 2019b. Point-Voxel CNN for efficient 3D deep learning. Adv. Neural Inform. Process. Syst. 963–973.

Malambo, L., Popescu, S., Horne, D., Pugh, N., Rooney, W., 2019. Automated detection and measurement of individual sorghum panicles using density-based clustering of terrestrial lidar data. ISPRS J. Photogramm. Remote Sens. 149, 1–13.

McCarthy, C., Hancock, N., Raine, S., 2009. Automated internode length measurement of cotton plants under field conditions. Trans. ASABE 52, 2093–2103.

McCormick, R.F., Truong, S.K., Mullet, J.E., 2016. 3D sorghum reconstructions from depth images identify QTL regulating shoot architecture. Plant Physiol. 172, 823–834.

Mei, J., Zhang, L., Wu, S., Wang, Z., Zhang, L., 2016. 3D tree modeling from incomplete point clouds via optimization and L1-MST. Int. J. Geograph. Inform. Sci. 31, 999–1021.

Méndez, V., Rosell-Polo, J.R., Pascual, M., Escolà, A., 2016. Multi-tree woody structure reconstruction from mobile terrestrial laser scanner point clouds based on a dual neighbourhood connectivity graph algorithm. Biosyst. Eng. 148, 34–47.

Miller, N.D., Haase, N.J., Lee, J., Kaeppler, S.M., Leon, N., Spalding, E.P., 2017. A robust, high-throughput method for computing maize ear, cob, and kernel attributes automatically from images. Plant J. 89, 169–178.

Moenning, C., Dodgson, N.A., 2003. Fast marching farthest point sampling for implicit surfaces and point clouds. Comput. Lab. Technical Report 565, 1–12.

Ninomiya, S., Baret, F., Cheng, Z.-M.M., 2019. Plant phenomics: emerging transdisciplinary science. Plant Phenom. 2019, 1–3.

Oosterhuis, D.M., Kerby, T.A., 2008. Measures of cotton growth and development. Crop Manage. Syst. 21, 1–6.

Paulus, S., Dupuis, J., Mahlein, A.-K., Kuhlmann, H., 2013. Surface feature based classification of plant organs from 3D laserscanned point clouds for plant phenotyping. BMC Bioinf. 14, 1–12.

Paulus, S., Schumann, H., Kuhlmann, H., Léon, J., 2014. High-precision laser scanning system for capturing 3D plant architecture and analysing growth of cereal plants. Biosyst. Eng. 121, 1–11.

Pieruschka, R., Schurr, U., 2019. Plant phenotyping: past, present, and future. Plant Phenom. 2019, 1–6.

Qi, C.R., Litany, O., He, K., Guibas, L.J., 2019. Deep Hough Voting for 3D Object Detection in Point Clouds. arXiv preprint arXiv:1904.09664.

Singh, A.K., Ganapathysubramanian, B., Sarkar, S., Singh, A., 2018. Deep learning for plant stress phenotyping: trends and future perspectives. Trends Plant Sci. 23, 883–898.

Stewart, J.M., Oosterhuis, D., Heitholt, J.J., Mauney, J.R., 2009. Physiology of cotton. Springer Science & Business Media.

Sun, S., Li, C., Paterson, A., Jiang, Y., Robertson, J., 2018. 3D computer vision and machine learning based technique for high throughput cotton boll mapping under field conditions, 2018 ASABE Annual International Meeting. Am. Soc. Agric. Biol. Eng. 1–10.

Tagliasacchi, A., Delame, T., Spagnuolo, M., Amenta, N., Telea, A., 2016. 3D Skeletons: A State-of-the-Art Report, Computer Graphics Forum. Wiley Online Library, pp. 573-597.

Tardieu, F., Cabrera-Bosquet, L., Pridmore, T., Bennett, M., 2017. Plant phenomics, from sensors to knowledge. Curr. Biol. 27, R770–R783.

Tewarie, P., van Dellen, E., Hillebrand, A., Stam, C.J., 2015. The minimum spanning tree: an unbiased method for brain network analysis. Neuroimage 104, 177–188.

Tian, J., Wang, C., Xia, J., Wu, L., Xu, G., Wu, W., Li, D., Qin, W., Han, X., Chen, Q., Jin, W., Tian, F., 2019. Teosinte ligule allele narrows plant architecture and enhances high-density maize yields. Science 365, 658–664.

Tilman, D., Balzer, C., Hill, J., Befort, B.L., 2011. Global food demand and the sustainable intensification of agriculture. Proc. Natl. Acad. Sci. 108, 20260–20264.

Vazquez-Arellano, M., Griepentrog, H.W., Reiser, D., Paraforos, D.S., 2016. 3-D imaging systems for agricultural applications-A review. Sensors 16, 1–24.

Wang, G., Laga, H., Xie, N., Jia, J.Y., Tabia, H., 2018. The shape space of 3D botanical tree models. ACM Trans. Graphics 37, 1–18.

Wu, S., Wen, W., Xiao, B., Guo, X., Du, J., Wang, C., Wang, Y, 2019. An accurate skeleton extraction approach from 3D point clouds of maize plants. Front. Plant Sci. 10, 1–14.

Xu, R., Li, C., Paterson, A., Jiang, Y., Sun, S., Robertson, J., 2017. Cotton bloom detection using aerial images and convolutional neural network. Front. Plant Sci. 8, 1–17.

Yamamoto, K., Guo, W., Ninomiya, S., 2016. Node detection and internode length estimation of tomato seedlings based on image analysis and machine learning. Sensors 16, 1–16.

Yin, X., Liu, X., Chen, J., Kramer, D.M., 2018. Joint multi-leaf segmentation, alignment, and tracking for fluorescence plant videos. IEEE Trans. Pattern Anal. Mach. Intell. 40, 1411–1423.